CrossMark

Suspended-Sediment Impacts on Light-Limited Productivity in the Delaware Estuary

Jacqueline M. McSweeney[1] · Robert J. Chant[1] · John L. Wilkin[1] ·
Christopher K. Sommerfield[2]

Abstract The Delaware Estuary has a history of high anthropogenic nutrient loadings but has been classified as a high-nutrient, low-growth system due to persistent light limitation caused by turbidity. While the biogeochemical implications of light limitation in turbid estuaries have been well-studied, there has been minimal effort focused on the connectivity between hydrodynamics, sediment dynamics, and light limitation. Our understanding of sediment dynamics in the Delaware Estuary has advanced significantly in the last decade, and this study describes the impact of spatiotemporal variability of the estuarine turbidity maximum (ETM) on light-limited productivity. This analysis uses data from eight along-estuary cruises from March, June, September, and December 2010 and 2011 to evaluate the impact of the turbidity maximum on production. Whereas the movement of the ETM is controlled primarily by river discharge, the structure of the ETM is modulated by stratification, which varies with both river discharge and spring-neap conditions. We observe that the ETM's location and structure control spatial patterns of light availability. To evaluate the relative contributions of river discharge and spring-neap variability to the location of phytoplankton blooms, we develop an idealized two-dimensional Regional Ocean Modeling System (ROMS) numerical model. We conclude that high river flows and neap tides can drive

✉ Jacqueline M. McSweeney
jmcsween@marine.rutgers.edu

[1] Department of Marine and Coastal Sciences, Rutgers, The State University of New Jersey, 71 Dudley Road, New Brunswick, NJ 08901, USA

[2] School of Marine Science and Policy, University of Delaware, Lewes, DE 19958, USA

stratification that is strong enough to prevent sediment from being resuspended into the surface layer, thus providing light conditions favorable for primary production. This study sheds light on the role of stratification in controlling sediment resuspension and promoting production, highlighting the potential limitations of biogeochemical models that neglect sediment processes.

Introduction

Light-limited production in estuaries has been a topic of much research in the last few decades. The Hudson Estuary (Stross and Sokol 1989), San Francisco Bay (Cloern 1991; May et al. 2003), the Chesapeake Estuary (Malone et al. 1988), and the Delaware Estuary (Pennock 1985; Fisher et al. 1988) all demonstrate light limitation. While the temporal and spatial patterns of light limitation vary between systems, the underlying physics controlling light availability are similar in these turbid estuaries. That is, light is attenuated by sediment, chlorophyll, chromophoric dissolved organic matter (CDOM), and the water itself. The distribution of these light absorbers is spatiotemporally variable, and light attenuation is therefore modulated by stratification, mixing, and circulation.

Suspended sediment has important implications in turbid estuaries with high nutrient loadings, where it may be the dominant factor limiting light available for primary production. Estuaries trap sediment from both riverine and coastal sources, and the estuarine turbidity maximum (ETM) zone, an area of elevated suspended sediment concentrations (SSCs), is a region of active sediment trapping, resuspension, and deposition. Because sediment suspended in the surface waters

attenuates light, low-light conditions can persist in high resuspension regimes (Biggs et al. 1983). Light limitation due to sediment ultimately depends on the frequency and duration of resuspension, particle size and density, and sediment concentration. The mechanisms that control sediment transport may vary spatially and temporally (Scully and Friedrichs 2007; Ralston et al. 2012; McSweeney et al. 2016), impacting the distribution of sediment within the estuary. Understanding the dynamics that control sediment distribution and resuspension is fundamental to understanding how the optical environment is modified, especially within an estuary's ETM.

While others have acknowledged the importance of light limitation in turbid estuarine and coastal systems (Desmit et al. 2005; Arndt et al. 2007; De Swart et al. 2009) and investigated the role of hydrodynamics influencing estuarine sediment and light fields (Lawson et al. 2007; Devlin et al. 2008; Ganju et al. 2014), we present field observations and idealized model runs to explain these mechanisms in greater detail with the specific goal of relating spatiotemporal variations in stratification to patterns of primary production. This study focuses on the linkages between hydrodynamics, sediment dynamics, and light limitation in the Delaware Estuary, highlighting the importance of river discharge and spring-neap variability. The underlying mechanisms we discuss are broadly applicable to turbid estuarine systems and could provide insight into lingering questions about light limitation.

Early modeling of light availability and chlorophyll in the Delaware estuary highlights that suspended matter is the primary regulator of light limitation and productivity under non-stratified conditions (Wofsy 1983). However, stratification can persist in the Delaware on both tidal and longer timescales. For instance, stratification on a tidal timescale is modulated by a combination of along-channel and across-channel processes such that the flood can be either more or less stratified than the ebb tide (Aristizábal and Chant 2014; McSweeney et al. 2016). There is also spring-neap variability of stratification, with neap tides more stratified than spring tides (Aristizábal and Chant 2014; McSweeney et al. 2016). High river discharge during the spring season also favors persistently stratified conditions, which have been observed to increase light availability and coincide with the initiation of phytoplankton blooms (Pennock 1985). Spatiotemporal patterns in stratification always impact primary production through modification of the mixed layer depth and therefore average light availability, but this analysis emphasizes that there is also an indirect effect of stratification on light due to interactions between stratification and suspended sediment. Recent advances in our understanding of stratification mechanisms (Aristizábal and Chant 2014) and sediment dynamics (McSweeney et al. 2016) provide insight about the spatial and temporal patterns of stratification and how they may impact the optical environment by modulating sediment resuspension.

Despite an abundance of anthropogenic nutrient input, the Delaware Estuary has been described as a high-nutrient, low-growth environment because the attenuation of light by turbidity limits primary production and suppresses excessive blooms (Sharp et al. 1986; Pennock 1987; Yoshiyama and Sharp 2006). Production is maximal down-estuary of ETM, but levels of production are seasonally variable, with low values in the winter compared to the spring (Biggs et al. 1983). Observations indicate that the upper, turbid reach of the estuary is light limited year-round, while the lower and mid-estuaries may not be light limited March through September (Pennock and Sharp 1994). The upper estuary, in the known vicinity of the turbidity maxima, is geochemically filtered such that certain constituents are removed by flocculation reactions. In comparison, the lower estuary is more driven by biochemical filtration and removal by organismic processes (Biggs et al. 1983; Sharp et al. 1984). However, high flushing rates in the upper estuary during the spring cause the residence time to become shorter than the chemical kinetics, decreasing the influence of geochemical filtration (Sharp et al. 1984) and the amount of flocculated material in the turbidity maximum.

While there have been many regional studies focused on light limitation and the feedbacks on productivity and biogeochemistry, the linkages between the sediment system itself and light availability are far less studied in the Delaware. Our understanding of sediment dynamics within the estuary has developed significantly in the last decade (Cook et al. 2007; Sommerfield and Wong 2011; McSweeney et al. 2016) and could provide important insight about spatiotemporal patterns of light limitation. Whereas previous studies have indicated that high nutrient loads in the Delaware do not elicit excessive blooms due to the lack of summer stratification caused by low river flows (Sharp et al. 2009), the present research emphasizes that the estuary has intermittent salinity stratification that effectively limits sediment resuspension enough to permit primary production.

The objective of this study is to examine linkages between sediment dynamics and optics in the Delaware Estuary to advance our understanding of the main controls on primary production. We aim to clarify the role of stratification in modulating surface SSC and light availability, which will improve our ability to model estuarine biogeochemical processes. Since estuarine dynamics are temporally variable, we examine the relative importance of river discharge and spring-neap variability to light-limited production. By drawing attention to the connection between the structure of the ETM and spatial patterns of phytoplankton biomass, this analysis ultimately provides interdisciplinary insight about the influence of estuarine dynamics on primary production in a turbid system.

Regional Background

The Delaware Estuary is a coastal plain estuary in the mid-Atlantic region. It extends approximately 215 km

from the mouth of the bay to the head of the tides near Trenton, New Jersey (NJ) (Fig. 1). The Delaware River has a mean annual discharge of 330 m^3 s^{-1} and is the main source of freshwater input to the estuary, followed by the Schuykill and Christina river tributaries, which contribute 77 and 19 m^3 s^{-1}, respectively. From the historic US Geological Survey discharge record, it is evident that discharge (Q_R) is typically maximal in March and minimal in September (Fig. 2). Suspended-sediment delivery increases with freshwater discharge, and thus, the highest sediment loadings to the system typically accompany the spring freshet. The sediment load in tons day^{-1}, Q_s, has been estimated as Q_s $a \cdot Q_R^b$, where a is 0.01 (tons day^{-1} m^{-3} s) and b is 1.8 for the Delaware River at Trenton (Nash 1994). The mean supply of all riverine sediment is estimated to be about 1–2 × 10^9 kg year^{-1} (Mansue and Commings 1974) and, using the rating relationship above, we estimate that the sediment loading at Trenton was 2.5 × 10^8 kg in 2010 and 7.3 × 10^8 kg in 2011. Notably, because 2011 was an anomalously wet year with several large storms, the sediment load in 2011 was nearly triple that of 2010.

The upper estuary bed is predominantly muddy compared to the sandy lower estuary (Delaware Bay), and the mid-estuary tends to be a mixture of sand and mud (Weil 1977; Biggs and Beasley 1988; Sommerfield and Madsen 2004). The NJ side is dominated by sands from the continental shelf, whereas the Delaware (DE) side is a mix of fluvial and coastal plain sources (Neiheisel 1973). Flocculation rates are maximal within the ETM region, and mudfloc sizes thus increase with proximity to the salt intrusion front; comparatively, the tidal river and lower bay tend to have lower SSC values and smaller particle aggregates (Gibbs et al. 1983).

The along-channel structure of the Delaware's ETM is such that the landward leading edge is characterized by sediment mixed throughout the water column whereas the interior (or tail) has sediment that is constrained to lower in the water column by stratification (McSweeney et al. 2016). In the lateral direction, sediment concentrations are consistently greater on the DE side of the estuary compared to the NJ side. Observations of sediment transport within the ETM region indicate that the ETM structure is laterally strained by tidal and subtidal processes that drive export on the DE flank and import within the channel (Sommerfield and Wong 2011; McSweeney et al. 2016).

The tidal freshwater Delaware River flows past the city of Philadelphia, which houses the fifth largest metropolitan population in the country (US Census 2010) and the Wilmington-Philadelphia port complex, one of the largest US shipping ports both historically and presently. Due to the level of urbanization, the estuary has extremely high nutrient loadings (Sharp et al. 2009). The chemical and biological response to high nutrient conditions has been monitored regularly since systematic sampling was initiated by Sharp et al. (1982),
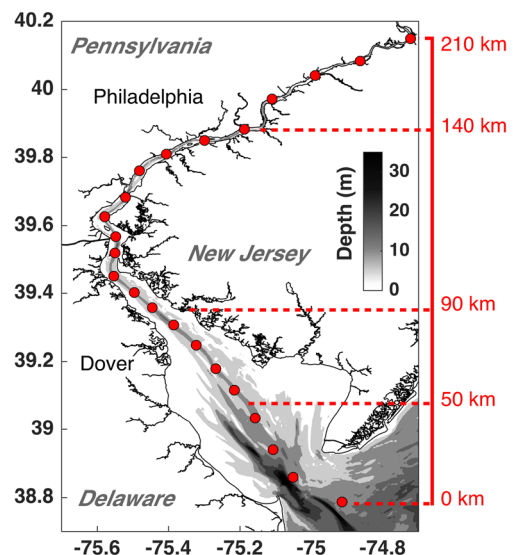
Fig. 1 Map of the Delaware Estuary with *grayscale depth* and *red dots* indicating the 23 stations included in the along channel surveys. The along channel distance (km) is noted in *red* right of the figure. The approximate locations of ocean, lower-estuary, mid-estuary, upper-estuary, and tidal river are 0–14, 14–50, 50–90, 90–140, and 140–210 km, respectively. Trenton is located in NJ just north of the northernmost station

resulting in the finding that Delaware Estuary, unlike the neighboring Chesapeake, does not experience episodes of eutrophication.

Methods

Observations

Along-estuary surveys were conducted in March, June, September, and December of 2010 and 2011. Conditions during each sampling period are listed in Table 1. Each survey took about 2 days, and there were 23 sampling stations along the thalweg from outside the mouth of the estuary to Trenton, NJ, spanning the ocean; the lower, mid-, and upper estuaries; and the tidal river (Fig. 1). Vertical profiles were taken at each station with an instrument package that included an RBR CTD sensor to measure temperature and salinity, an optical back-scatter (OBS) sensor, a Chelsea Aquatraka fluorometer, an Aanderra Optode oxygen sensor, and a Satlantic SUNA nitrate sensor. A shipboard flow-through fluorometer also collected fluorometry data at the surface.

Chlorophyll concentrations were estimated from the profiling fluorometer using the instrument's factory calibration. Due to instrument issues with the profiling fluorometer, we only had surface fluorometry data from the ship-mounted fluorometer in March 2010. To maintain consistency with the chlorophyll estimations, we calibrated the June 2010 profiling and boat-mounted fluorometers against each other and
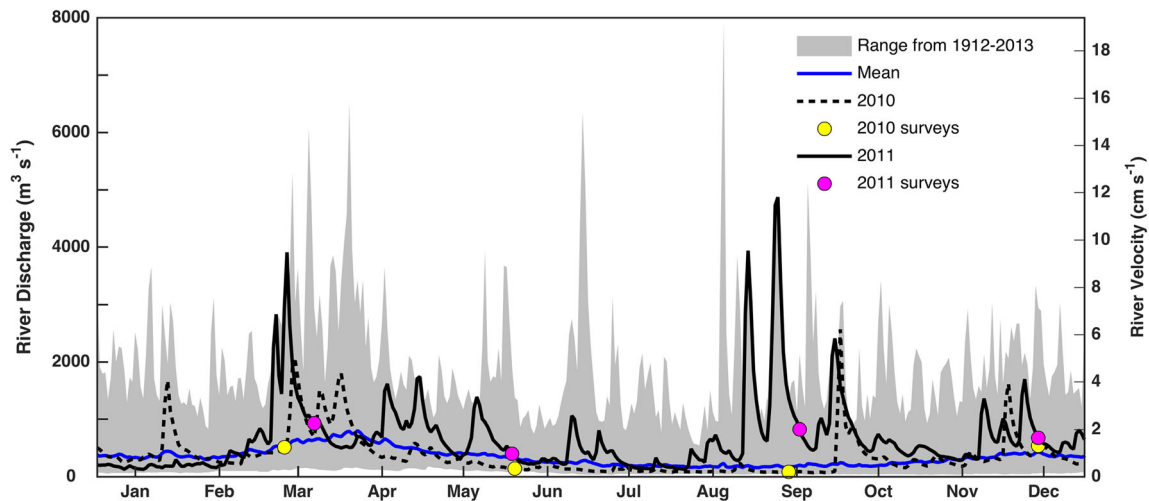
Fig. 2 USGS River discharge data from 1912 to 2014 plotted by yearday. The *gray* shaded region is the range of historic data, the *blue line* is the historic mean, the *dotted black line* is the 2010 record, the *solid black line* in the 2011 record, and the *yellow* and *purple dots* indicate the discharge conditions during the 2010 and 2011 along-channel surveys respectively. The right y-axis is the river velocity (cm s^{-1}), which is the river discharge divided by the approximated cross-sectional area in the vicinity of the ETM

used this calibration to calibrate the March 2010 boat-mounted fluorometer.

Water samples were collected with a pump 1 m below the surface and 0.5 m above the bed at each station. These samples were filtered to yield suspended sediment concentrations (SSC, mg L^{-1}). The OBS was then calibrated to SSC following the methods described by Kineke and Sternberg (1992).

Vertical profiles of downward-irradiance were collected with a profiling radiance radiometer 600 (PRR) from Biospherical Instruments Inc. PRR cast depths were dependent on the irradiance penetration and typically ranged between 5 and 7 m. PRR casts were only done during daylight, leading to limited spatial sampling during some cruises. Due to instrument issues, we were unable to collect optical data in September 2010 and June 2011.

The PRR collected data at six specific wavelengths, so photosynthetically active radiation (PAR) was calculated by approximating the integral of the spectrum from 400 to 700 nm using the following equation:

$$PAR = \sum_{i=1}^{n} I_1 \Delta \lambda_1 + I_2 \Delta \lambda_2 + ... + I_n \Delta \lambda_n \approx \int_{400}^{700} I(\lambda) \partial x \quad (1)$$

where I is the light intensity of a given wavelength λ. The depth-varying light attenuation can be described by

$$\alpha(z) = \frac{\partial I}{\partial z} \cdot \frac{1}{I_{avg}} \tag{2}$$

where α is the diffuse absorption coefficient, z is the depth, and I_{avg} is the average irradiance at a given depth. For a constant α, the solution for Eq. 2 is an exponential profile.

Table 1 Conditions during each field-sampling period

Dates	Tidal conditions	River discharge (m^3 s^{-1})	Sediment inventory (metric ton m^{-1})	Notes
11–12 March 2010	Neap	513	83	
3–4 June 2010	Neap	143	84	
12–13 Sept 2010	Spring	86	122	Extremely dry period
13–14 Dec 2010	Neap	688	135	
21–22 March 2011	Spring	932	266	Days after a big discharge event
3–4 June 2011	(weak) Spring	402	97	
16–17 Sept 2011	Neap	827	92	Days after Tropical storm Lee
13–14 Dec 2011	Neap	680	172	

The diffuse absorption coefficient can be further decomposed to isolate the attenuating factors important in estuarine systems:

$$\alpha = \alpha_{sw} + \alpha_{chl}[Chl] + \alpha_{\mathrm{CDOM}}[\mathrm{CDOM}] + \alpha_{sed}[SSC] \qquad (3)$$

where α_{sw} is the absorption due to seawater; α_{chl}, α_{CDOM}, and α_{sed} are the specific absorption coefficients for chlorophyll, CDOM, and sediment respectively; and $[Chl]$, $[CDOM]$, and $[SSC]$ are the concentrations of chlorophyll, CDOM, and suspended sediment (Gallegos et al. 2005). Because CDOM has been found to minimally impact light attenuation in the turbid salinity reach of the Delaware estuary (Sharp et al. 2009), we neglect the $\alpha_{CDOM}[CDOM]$ term in Eq. 3 to focus on the dynamics within the turbidity maximum. We estimate the α_{sw}, α_{chl}, and α_{sed} by iteratively minimizing the root mean squared error (RMSE) between the observed irradiance profiles and the modeled irradiance solution, which relies on measurements of chlorophyll and SSC along with initial best estimates for α_{sw}, α_{chl}, and α_{sed}. The best-fit coefficients are listed in Table 2, along with values from the literature for comparison.

Notably, our estimate for α_{sw} is high compared to values in the literature due to the inclusion of data from the tidal fresh reach and neglect of CDOM. Whereas Sharp et al. (2009) concluded that CDOM was a relatively unimportant attenuator in the salty regions of the estuary, they found it to be more important in the fresh tidal reach. Our analysis focuses on the dynamics within the ETM rather than those in the fresh reach, but we include the data from all the transects in our estimation of the attenuation coefficients to best estimate irradiance throughout the entire estuary. Because we did not measure CDOM, we could not calculate α_{CDOM}. Rather, the effect of CDOM was folded into the estimate of α_{CDOM}, in effect inflating it. Despite this, attenuation due to sediment dominated within the ETM and the likely overestimate of α_{sw} had little effect there. Results in the tidal fresh reach, in contrast, entail more uncertainty due to the influence of CDOM but are not the focus of this analysis.

The estimated sediment and seawater coefficients were then used as inputs in the idealized ROMS model described in the "Idealized Model" section. We selected to use the chlorophyll-specific attenuation from Pennock (1985) to parameterize the ROMS model rather than use our estimate, which was based on fluorescence calibrations rather than direct observations, because ROMS models chlorophyll biomass, not fluorescence.

Idealized Model

We use a regional ocean modeling system (ROMS) hydrodynamic model (Haidvogel et al. 2000; Shchepetkin and McWilliams 2005) coupled with a biogeochemical model (Fennel et al. 2006) and the community sediment transport modeling system (CSTMS) sediment model (Warner et al. 2008) to investigate the impacts of the sediment on light-limited production in an idealized estuary. The model is quasi-2D, focusing on the along-estuary direction without the influence of changing estuary width, lateral bathymetry, or lateral circulation. Since the spatial sediment and chlorophyll patterns in the Delaware have been observed to have a strong along-channel signal, we use the two-dimensional framework to focus on the axial processes. The turbidity maximum indeed has important three-dimensional structure (McSweeney et al. 2016), and, as discussed further in the "Spring-Neap Variability" section, the importance of lateral processes is something to explore in future work.

The model estuary is 150 km long (200 grid points) and 500 m wide (7 grid points) with a depth that linearly decreases from 15 m at the mouth to 4 m at the head. There are 20 vertical terrain-following coordinate layers stretched to weight resolution toward the surface and bottom boundary layers. The sides and head of the estuary are closed boundaries, and the mouth is an open boundary with combined radiation and nudging conditions (Marchesiello et al. 2001) for nitrate,

Table 2 Optical properties estimated from data (as described in the "Observations" section) compared to those in the literature

Parameter	Symbol	Value	Reference
Incoming shortwave radiation below the sea surface (W m^{-2})	I_0	**340**	
Fraction of shortwave radiation that is photosynthetically active	par	**0.43**	
Attenuation coefficients for estuarine water (m^{-1})	α_{sw}	0.095	Pennock (1985)
		0.40	This study
Attenuation coefficients for chlorophyll (m^{-1}/(mg L^{-1}))	α_{chl}	0.020	Pennock (1985)
		0.050	This study
Attenuation coefficients for sediment (m^{-1}/(mg L^{-1}))	α_{sed}	0.075	Pennock (1985)
		0.0589	Arndt et al. (2007)
		0.065	This study

The values that are bolded were used to parameterize the idealized ROMS model

oxygen and temperature, and radiation conditions (Orlanski 1976) for all other tracers. Chapman/Flather conditions are used for sea level and depth-average velocity in conjunction with imposed tidal variability in the form of a simple harmonic progressive wave. A gradient condition is used for 3D momentum. We use the generic length scale (GLS) $k - \varepsilon$ vertical turbulence closure scheme (Umlauf and Burchard 2003) and a constant quadratic bottom drag coefficient.

The base model includes M_2 tides and Coriolis, but no wind. In order to address the role of spring-neap variability, we also run a case of constant river discharge (75 m^3 s^{-1}) that has M2 and S2 tidal constituents of equal magnitude. The spring-neap case is discussed in Section 4.4. Each model run has a constant river discharge, which will be discussed further in the "The Role of River Discharge" section. The model is initialized using vertically well-mixed fields for nitrate and salinity that have a constant gradient along the channel, and then nitrate, oxygen, and sediment are all delivered with a point source riverine input at the head. The delivery of nitrate, oxygen, and sediment is constant and independent of river discharge, so that the river discharge model

simulations compare only varying physics. Because there is an excess of nutrients, nitrate supply is not a limiting factor for production in any of the discussed cases.

The sediment model includes three non-cohesive sediment classes, and there are two active bed layers that vary in thickness depending on the history of erosion and deposition, as described by Warner et al. (2008). In the Delaware, suspended-sediment characteristics in the vicinity of the ETM vary from those in the lower bay. Because production is most often light limited in the region of the turbidity maximum, the model is designed to represent the sediment dynamics in this region. Consequently, we initialize the model with a Gaussian distribution of sediment that is centered in the expected vicinity of the ETM and prescribed sediment characteristics typically of those observed in the Delaware's ETM (described in Table 3).

In the biogeochemical model described by Fennel et al. (2006), phytoplankton growth depends on the available PAR, which is controlled by light attenuation from the seawater and chlorophyll. To include the absorption by sediment, we modify the equation for the absorption of photosynthetically available radiation (I) as follows:

$$I = I(z) = I_o \cdot \text{par} \cdot \exp\left\{-\left(\alpha_{sw} + \alpha_{chl}\int\limits_z^0 \text{Chl}(\sigma)\partial\sigma + \alpha_{sed}\int\limits_z^0 \text{SSC}(\sigma)\partial\sigma\right) \cdot z\right\} \tag{4}$$

where I_0 is the incoming light in the surface water, par is the fraction of light photosynthetically available, Chl(σ) and SSC(σ) are the chlorophyll and suspended sediment concentrations at sigma layer σ, and z is depth. The constants α_{sw} and α_{sed} are iteratively estimated as described in the "Observations" section, and we use α_{chl} from Pennock (1985) (Table 2). We run two sets of simulations with different α_{sed} values to compare our estimation (0.065 m^{-1}/(mg L^{-1})) with that by Pennock (1985) (0.075 m^{-1}/(mg L^{-1})), though (as discussed in the "Implications for Modeling Primary Productivity" section) we only show results from the models with $\alpha_{sed} = 0.065$ m^{-1}/(mg L^{-1}) because the model is insensitive to the two different values.

Results and Discussion

Light Limitation Due to Sediment

In June 2010, the observed along-channel suspended-sediment concentrations are greatest near the salt front (Fig. 3a). Here, the water column is well-mixed and resuspended sediment reaches the surface layer. SSCs are also elevated roughly

20 km down-estuary of the salt front, though the resuspension does not reach as high in the water column due to stratification. Within the vicinity of the ETM, light absorption by surface sediment causes the 1% light level to be very shallow—approximately 3 m below the sea surface (Fig. 3b). Chlorophyll concentrations are maximal up- and down-estuary of the ETM, where light penetrates deeper. Observations of nitrate and oxygen provide supporting evidence that primary production is occurring in these regions, as the highest chlorophyll concentrations coincide with an uptake of nitrate and the production of oxygen (Fig. 3c, d). Primary production appears to be shut down in the vicinity of the ETM where light levels are lowest, and the minimal oxygen levels indicate respiration.

The nitrate signal in Fig. 3c is consistent with that reported by Sharp et al. (2009), who found nitrate to be high at the head of the tide, increase in the reach of the urban river, and then decrease toward the mouth due to dilution with coastal ocean water. While our observations are consistent with this described pattern and the depletion of nitrate toward the mouth may reflect some dilution with coastal water, we posit that the coincidence of nitrate depletion, oxygen production, and increased chlorophyll biomass is also indicative of uptake due to primary

Table 3 Model sediment properties

Settling velocity (mm s^{-1})	Erosion rate (kg m^2 s^{-1})	Critical stress for erosion (N m^{-2})	Critical stress for deposition (N m^{-2})
3.0	5×10^{-4}	0.05	0.10
8.0	5×10^{-4}	0.05	0.10
10.0	5×10^{-4}	0.05	0.10

production. To confirm this, we plot the nitrate-salinity relationship from all the June 2010 casts against the theoretical conservative mixing curve (Fig. 4). The concave deviation from conservative mixing is consistent with that predicted for biogeochemical filtration (Sharp et al. 1984), indicating that nitrate is being removed by biological uptake.

To quantify the relationship between sediment concentration and light absorption, we use a light-attenuation model based on sediment and chlorophyll observations and our estimations of the specific attenuation coefficients (described in the "Observations" section). Figure 5 shows profiles of modeled and observed irradiance for June 2010 and the model-observation comparison for all data from June 2010 and September 2011. We specifically plot the mid-bay and upper profiles from June 2010 (Fig. 5a) to illustrate that the fit can either overestimate or underestimate irradiance in the upper 1 m of the water column, but that there is strong

agreement between the model and observation below 1 m depth. We note, though, that the upper and mid-profiles shown in Fig. 5a are not representative of all profiles in those vicinities; we show the poorer fits to illustrate the possible error, but most of the profiles have a better fit.

Despite uncertainties in the light-attenuation model, the main conclusions of this analysis are robust. Sensitivity analyses confirm that described sediment-light paradigm holds true for the range of model parameters detailed in Table 3.

The Structure and Location of the Turbidity Maximum and Consequences for Productivity

The position of the salt intrusion front and the location of the ETM are modulated by river discharge (Fig. 6), which generally has a seasonal cycle (Fig. 2). During high river discharge, such as during December 2010 and 2011, the salt front and ETM move oceanward. In contrast, during low discharge, the salt front and ETM migrate landward, as is seen in the June months. Since the salt front has a faster response time to river discharge changes, the movement of the ETM can lag such that the ETM is temporarily not colocated with the salt front. For example, in September 2011, a large discharge peak pushed the salinity front down-estuary but the ETM had not yet migrated oceanward (Fig. 6).
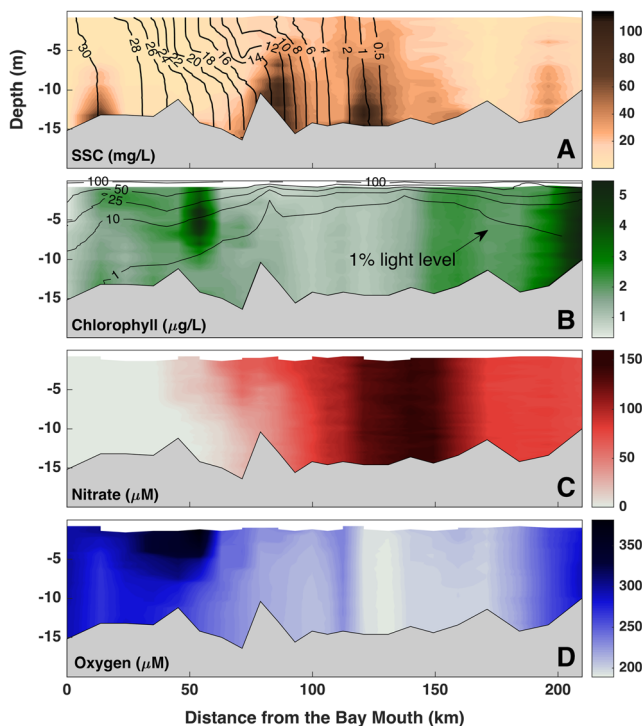

Fig. 3 June 2010 along channel distribution of sediment (mg/L), chlorophyll (μg/L), nitrate (μM), and dissolved oxygen (μM). *Black contours* in *top panel* are salinity and contours in *second panel* are PAR as a percentage of that at the surface
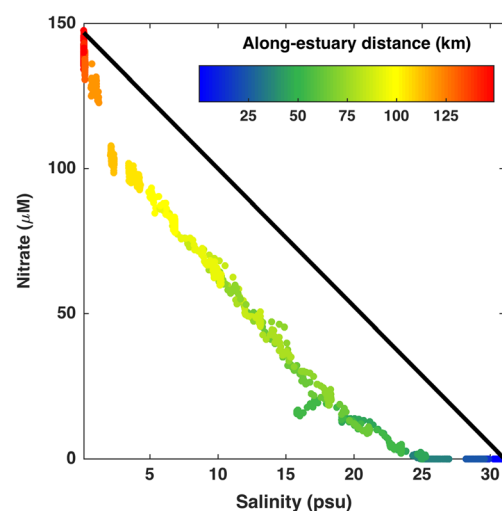
Fig. 4 Nitrate concentrations (μM) versus salinity (psu) for the June 2010 cruise (*dots*) colored by the along-estuary distance compared to the theoretical conservative mixing curve connecting the high and low nitrate endpoints (*black line*)

Fig. 5 **a** The observed irradiance profiles (*solid lines*) and the modeled irradiance profiles derived from Eq. 3 (*dotted lines*) for locations in the lower (*black*), mid (*red*), and upper (*blue*) estuary in June 2010. **b** The modeled irradiance versus the observed irradiance for all June 2010 and September 2011 data
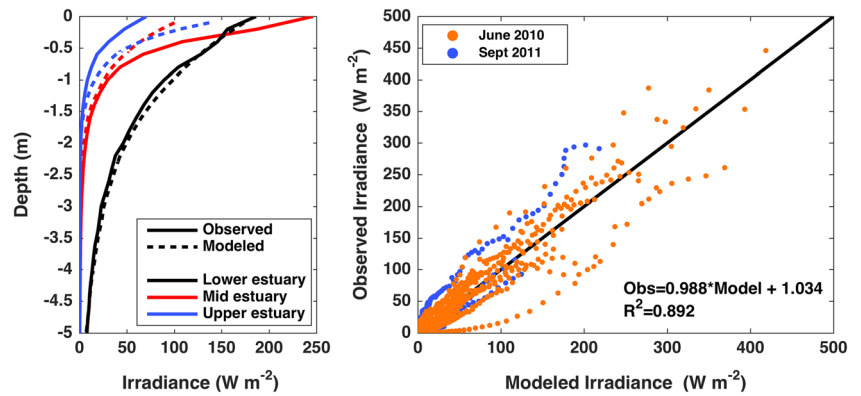
Stratification conditions, which are modulated by both river discharge and spring-neap variability, play an important role in regulating the structure of the ETM. Whereas neap tides and high river flows drive more stratified conditions, the estuary tends to be well-mixed during low flow and spring tides. Though stratification in the Delaware Estuary is usually very weak during spring tides, high river flows can drive persistent stratification even during spring tides (Aristizábal and Chant 2014). At the leading landward edge of the salt front and ETM, the water column is often well-mixed and sediment is resuspended throughout the entire water column. In the interior (or tail) of the ETM, resuspension is most often limited to lower in the water column by stratification. This ETM structure is particularly evident in March, June, and December of both 2010 and 2011.

The ETM structures in September 2010 and 2011 are more variable due to the combinations of river and tidal conditions. In September 2010, low river flows and spring tides result in mixed conditions throughout the estuary, which cause sediment in the ETM to be resuspended through the entire water

column. In September 2011, high river flows and neap tides result in strongly stratified conditions and the ETM is not aligned with the salt front. Because the September 2011 data was collected just days after Tropical Storm Lee and it is known that the ETM response time to discharge events can be lagged compared to salinity, we posit that the ETM had not yet migrated oceanward in response to the discharge event. However, realistic modeling would be required to confirm this. Sediment cores after Tropical Storm Lee indicate that the bed in the tidal river was scoured and that there was rapid deposition downstream of the salt wedge after the event (Duval 2013). Thus, it is likely that the sediment observed landward of the salt intrusion was remobilized recently from the tidal river. Because river discharge conditions in September are typically similar to those in 2010 (Fig. 2), we suggest that the along-channel salinity and ETM structure in 2010 is more representative of a typical September in the absence of tropical storms.

Because Fig. 6 shows data collected from 2-day surveys, some of the turbidity structure may be associated with tidal
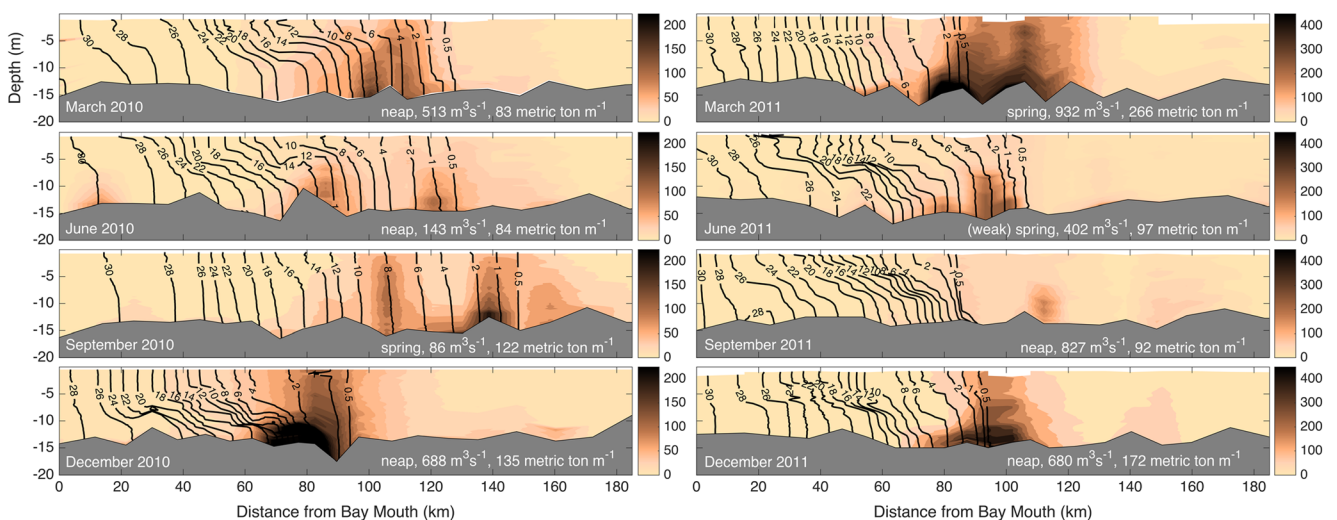
Fig. 6 Suspended sediment concentrations (mg/L) for the eight surveys with salinity contoured in *black*. The spring-neap conditions, river discharge, and sediment inventory for each survey are noted in the bottom right of the panels and also in Table 1

aliasing. However, the range of spring-neap tidal conditions that are encompassed in the observations (noted in Table 1) along with the consistency of the observed ETM structures provide confidence that our results are robust. Stratification plays an important role in limiting the height of resuspension, particularly in the tail of the ETM, and Fig. 6 clearly illustrates that the structure of the salt field coincides with the height to which sediment is resuspended. For example, in June 2010, sediment in the oceanward part of the ETM is trapped below the 12 psu isohaline due to stratification. The seasonal cycle of river discharge and spring neap-variability clearly impacts the surface SSC in the ETM through stratification, which has direct implications on the light availability and consequent biogeochemical processes.

Since primary production occurs at the water surface, the temporal sediment pattern at the surface is ultimately important. Figure 7 highlights sediment concentration, stratification, and chlorophyll concentrations 1.5 m below the surface as a function of river distance for the March, June, September, and December months. The consistency of the 2010 and 2011 surface data indicates that the sediment and stratification patterns are seasonal features. Surface sediment concentrations are highest in March and December, with notably heightened concentrations that coincide with river discharge peaks. Though high river flows drive strong stratification, the leading edge of the salt intrusion remains well-mixed even during these discharges and sediment is resuspended into the surface layer (Fig. 6). Thus, the heightened sediment supply in March and December months is evident in the surface sediment concentrations (Fig. 7).

The seasonality of stratification and surface SSC implies that spatial patterns of light attenuation also generally have a seasonal cycle. As such, light-limitation would spatially coincide with the ETM and the light environment would be more conducive to production down-estuary of the ETM. Indeed, we observe that, aside from December when there are light and temperature limitations, the chlorophyll maximum is persistently found down-estuary of the ETM. This finding is consistent with historical observations (Pennock 1985). There is also a chlorophyll peak up-estuary of the ETM in June, which we posit is likely due to a combination of elevated short-wave radiation and flushing rates that are slow enough for significant biomass to accumulate. Flushing times in the upper estuary, which is quite narrow, are sensitive to river discharge (Ketchum, 1952), resulting slow flushing rates during the dry months (Fig. 2). Chlorophyll concentrations are highest in March and minimal in December. The March chlorophyll maximum is consistent with the notion that stratification induced by the spring freshest limits sediment from being resuspended to the surface and permits the initiation of the spring bloom in the surface mixed layer. Though the discharge conditions similarly stratify the water column in the winter
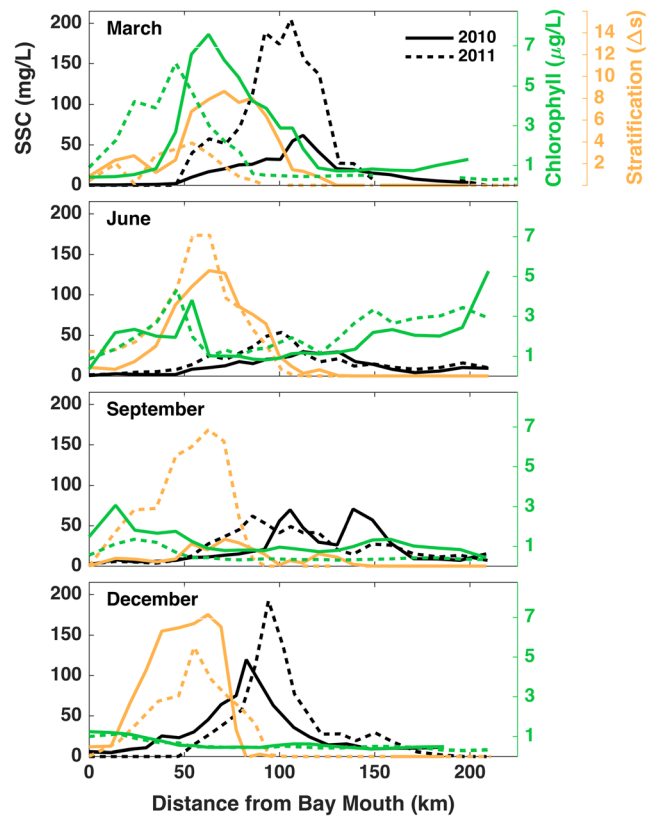
Fig. 7 Suspended sediment concentration (*black lines*) 1.5 m below the surface, chlorophyll (*green lines*) 1.5 m below the surface, and stratification (bottom salinity-surface salinity, *yellow lines*) for 2010 (*solid lines*) and 2011 (*dashed lines*). This data was collected along the estuary thalweg, following the track shown in Fig. 1

(Fig. 6), there is significantly less sunlight in December to support productivity.

Our observations shed light on the seasonality of the physics that modulate the light environment, but the seasonality of the blooms themselves are a function of light availability, and a number of factors not discussed here, such as temperature and grazing pressure. Our goal is to describe the role of stratification in influencing the bloom, which will likely modulate the perhaps larger seasonal scale variability associated with sunlight, temperature, and grazing. Thus, our results provide context on the physics that control estuarine productivity in turbid estuaries and suggest that variability in seasonal production would be modulated primarily by river discharge and secondarily by spring-neap stratification.

The Role of River Discharge

To better understand how river discharge contributes to movement and structure of the ETM, we run a series of idealized ROMS models with different constant discharge values. The initial simulations are forced with M2 tidal currents on the order of 1.0 m s^{-1}, so spring-neap variability is not an

Fig. 8 Model steady-state average solution (model day 30–60) from a run with a river discharge of 75 m^3 s^{-1}. Same layout as Fig. 3
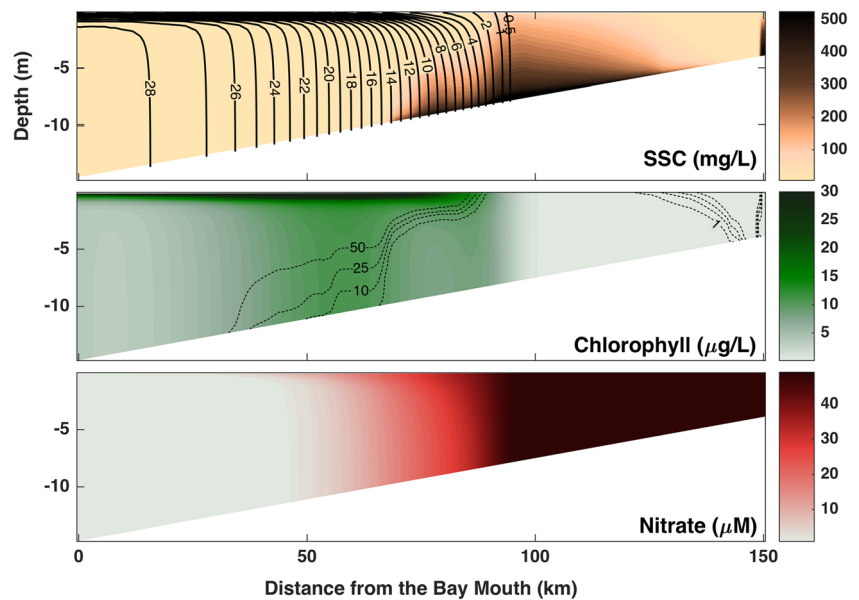
influence. The simulations reach steady state after about 30 model days, and Fig. 8 shows the steady-state average solution (model day 30–60) for a run with 75 m^3 s^{-1} constant river discharge. Details of the ETM structure differ from the observations (Fig. 6) which is unsurprising given the many differences between the idealized model geometry and reality. But the ETM still has the key features of resuspension through the entire water column near the well-mixed salt front, while resuspension is constrained to a lower layer downstream where stratification is important. Notably, the stratification is much shallower than observed in the estuary, so the tail of the ETM, roughly between 70 and 80 km up-estuary from the bay mouth, extends higher in the water column.

The chlorophyll concentrations are highest down-estuary of the turbidity maximum where stratification prevents sediment from reaching the surface. Chlorophyll is most concentrated in the surface layer, but some biomass is mixed down along the isopycnals. Production is notably low up-estuary of the ETM due to a combination of light limitation from the riverine sediment input and fast flushing times. The coincidence of the spatial patterns of sediment, chlorophyll, and production within the ETM is direct evidence that the structure of the suspended-sediment concentration field directly affects primary productivity.

Nitrate is depleted down-estuary of the turbidity maximum (Fig. 8), and the modeled nitrate-salinity curve (Fig. 9), colored by nitrate uptake and denitrification, confirms that nitrate is depleted from the system due to primary production. The nitrate curve indicates that the along-estuary nitrate distribution is controlled by uptake in addition to conservative mixing, verifying that the model is capturing nitrate dynamics similar to those observed (Fig. 4). As the model assumes that detritus instantaneously remineralizes when it hits the bed, the nitrogen removed by

denitrification was previously removed from the nitrate pool by uptake. The removal of nitrogen by nitrate uptake is an order of magnitude larger than that by denitrification and is greatest slightly up-estuary of the denitrification peak.

To evaluate how these spatial patterns are influenced by river discharge, we look at the along-channel distributions for six runs with constant river flows of 50, 75, 100, 125, 150, and 175 m^3 s^{-1}. These discharge values were chosen because the coinciding locations of the salt front and ETM are consistent within space with the observed range. However, the discharge values cannot be directly compared with observed discharge ranges due to the difference in the model's cross-sectional area and that of the bay. In order to draw a more direct comparison between the model and observations, we calculate the river velocities, U_R, in the vicinity of the ETM by dividing the river discharge by the cross-sectional area. The observed river velocities (Fig. 2, right y-axis) are slightly weaker than those modeled (Fig. 10, right y-axis), but the values are comparable.

Figure 10 shows the surface salinity, stratification, SSC, chlorophyll, and primary production as a function of along-estuary distance. As expected, the salt front moves down-estuary as the river discharge increases (Fig. 8a). The modeled salt intrusion length scales with $Q^{-1/3}$ (black dots), which is consistent with classic estuarine theory (Hansen and Rattray 1965; Monismith et al. 2002). The Delaware's salt intrusion length has been found to be less sensitive to discharge ($L \sim Q^{\approx -0.15}$) due to the tidal oscillatory salt flux, variability in the vertical eddy viscosity, and bathymetry (Aristizábal and Chant 2013), so the model is not capturing dynamics explicitly specific to the Delaware.

The stratification increases with increasing discharge (Fig. 10b), which is consistent with theory (MacCready

Fig. 9 Modeled nitrate-salinity curve from the steady-state average solution (model day 30–60) of the 75 m³ s⁻¹ simulation. Nitrate and salinity values are depth-averaged. On the left, the *dots* are colored by the depth integrated nitrate uptake (mmol N m⁻² day⁻¹). On the right, *dots* are colored by denitrification (mmol N m⁻² day⁻¹)
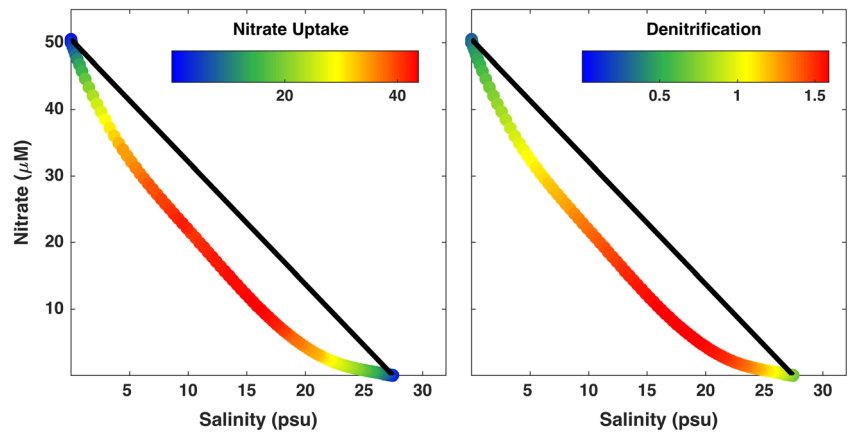
and Geyer 2010) and findings that the Delaware is most strongly stratified during the spring freshet. Stratification is minimal at the leading edge of the salt intrusion in every case and peaks about 5 km downstream of the salt intrusion. Notably, the reach of the strongest stratification also increases with increasing river flow, spanning roughly 25 km in the 50 m³ s⁻¹ case and 50 km in the 175 m³ s⁻¹ case.

Suspended sediment concentrations at the surface (Fig. 10d) are always greatest just up-estuary of the salt front. In every river flow case, there is a sharp transition to no sediment in the surface mixed layer that coincides with stratification. As river flow increases, the concentrations of resuspended sediment increase due to stronger flows. The sediment concentrations at the surface are roughly a third of those at the bed, as is seen in observations.

Fig. 10 Steady-state averaged model results (model day 30–60) for simulations with six different river discharges—50, 75, 100, 125, 150, 175 m³ s⁻¹. The 1-psu surface isohaline is drawn in each panel for reference. **a** The along-channel surface salinity (psu) with specific isohalines contoured and the theoretical salt intrusion length based on L ~ Q⁻¹ᐟ³ (*black dots*). **b** The stratification (bottom salinity-surface salinity); **c** the sediment concentration (mg L⁻¹) at the surface; **d** the chlorophyll concentration (μg L⁻¹) at the surface; **e** the surface new primary production (mmol N m³ day⁻¹)
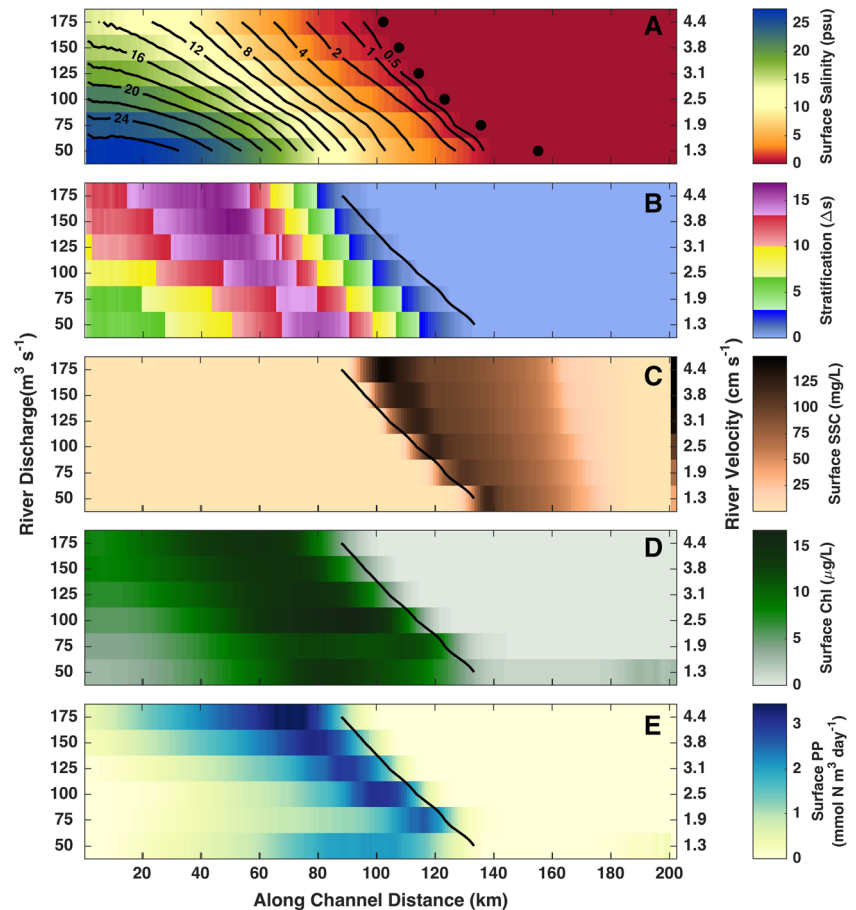
Unsurprisingly, the chlorophyll peaks move oceanward with increasing river discharge (Fig. 10e). Chlorophyll concentrations are nearly zero near the salt intrusion front where sediment reaches the surface. Just down-estuary, where light becomes available due to sediment being trapped below the surface mixed layer by stratification, a bloom is initiated. Chlorophyll concentrations then accumulate with distance down-estuary, as production continues and chlorophyll biomass is moved oceanward. Chlorophyll concentrations are slightly elevated up-estuary of the turbidity maximum in the low-flow case, which is consistent with the chlorophyll distribution observed in the June months.

Primary production is greatest in the stratified reaches of the estuary, just oceanward of the turbidity maximum for all river discharge cases. Primary production rates tend to decrease further down-estuary (Fig. 10d), where nutrients are less abundant. In the lower discharge case, there is weak production up-estuary that coincides with a chlorophyll peak similar to that observed in the June cruises.

Estuarine circulation inherently controls the steady-state solutions shown in Fig. 10. For example, the estuarine circulation plays a key role in modulating the location of the salt front (Hansen and Rattray 1965) and consequently the ETM. The axial sediment distribution is modulated by estuarine processes, as convergent fluxes trap sediment within the ETM region. The depth-integrated sediment flux in the ETM is relatively weak, and vertical mixing on a tidal timescale controls the surface SSC signal in the ETM and therefore the light attenuation. The location of primary production is controlled by the estuarine physics that modulate light availability, but the resulting chlorophyll biomass will be advected down-estuary at the surface due to the vertical structure of the riverine and estuarine exchange velocities. The spatial scale of this advection is visible in the comparison of Fig. 10d, e.

Spring-Neap Variability

While river discharge appears to modulate the spatial patterns of stratification, sediment, light-limitation, and productivity on a subtidal timescale, it is also possible that spring-neap variability can enhance or mask river-driven variability. The salinity front, stratification, and ETM position are known to vary on spring-neap timescales (Aristizábal and Chant 2014; McSweeney et al. 2016), and these signals can be of a similar magnitude as those caused by riverine influence Thus, we conduct a further simulation that includes M2 and S2 tides to tease apart the relative contributions of river discharge and spring-neap conditions.

Stratification is modified significantly on a spring-neap timescale, with the water column more strongly stratified during neap tides compared to spring tides (Fig. 11b). Correlated with stratification, modeled sediment concentrations in the
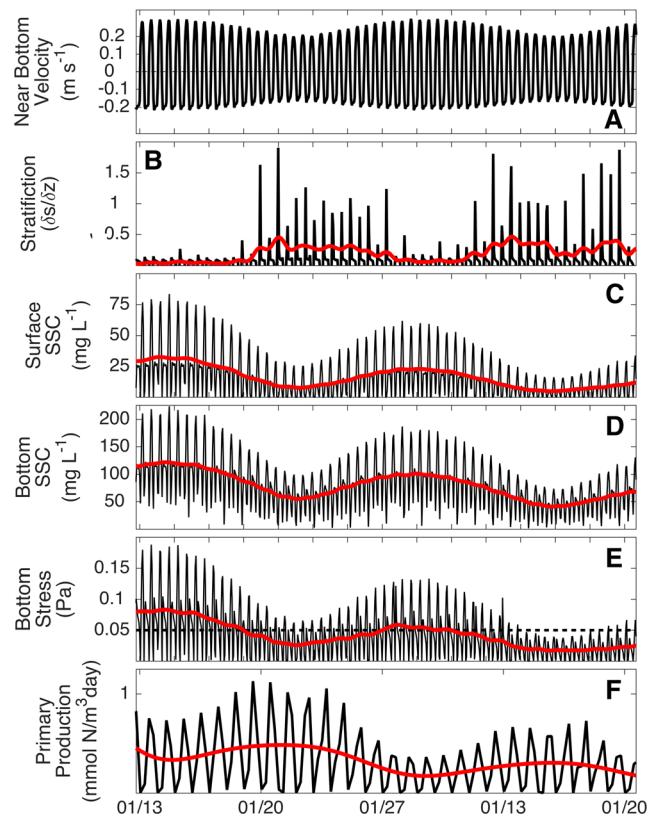
Fig. 11 Model output at a location 100 km from the mouth in the middle of the channel over a spring-neap cycle from a simulation with a constant river discharge. **a** The near-bottom velocities at a location near the salt intrusion. **b** The depth-averaged stratification, calculated by the difference in top and bottom salinity at each vertical level. **c** the surface SSC (mg L^{-1}). **d** The SSC a meter above the bed (mg L^{-1}). **e** The bottom stress (Pa) at the bed compared to the critical erosion stress (dashed line). **f** The primary production rate (mmol N m^{-3} day^{-1}). The low-pass filtered data are plotted in *red*

surface waters during spring tides are roughly double those during neap tides (Fig. 11b, c). Stratification and bottom stress are related through the vertical buoyancy frequency and the Simpson number:

$$N^2 \approx \frac{g\beta\left(\frac{\partial s}{\partial z}\right)}{H} \tag{5}$$

$$Si = \frac{g\beta\left(\frac{\partial s}{\partial x}\right)H^2}{u_*^2} \tag{6}$$

where N is the vertical buoyancy frequency, g is the acceleration due to gravity, β is the saline expansivity, $\left(\frac{\partial s}{\partial z}\right)$ is the tidally averaged vertical salinity gradient, H is the water depth, Si is the Simpson number, $\left(\frac{\partial s}{\partial x}\right)$ is the tidally-averaged horizontal salinity gradient, and u_* is a scale for bottom friction

velocity (Simpson et al. 1990; Stacey et al. 2001; Burchard et al. 2011). Thus, the reduction of bottom stress during the stratified neap tides (Fig. 11e) is consistent with theory. Modeled sediment concentrations a meter above the bed are consequently reduced during neap tides due to weakened bed stresses and increased stratification (Fig. 11d). Since surface SSC directly impacts light attenuation, there is a nearly two-fold increase in production that coincides with the increased stratification, reduced bed stresses, and lower surface SSC during neap tides (Fig. 11f).

Notably, bottom stresses during the neap tide at the end of January were below the critical erosion stress and yet there was still a significant amount of sediment suspended a meter above the bed. This sediment is material that was resuspended during more energetic conditions, either locally or in a more energetic location, and has not yet settled to the bed. This demonstrates that the sediment inventory in the water column is not necessarily entirely composed of newly resuspended sediment. This suggests that, while spring-neap variability of bottom stress definitely contributes to sediment resuspension, spring-neap variability of stratification is the main control on surface SSC. However, further work would be required to quantify the relative roles of bed stress and stratification in modulating surface sediment concentrations.
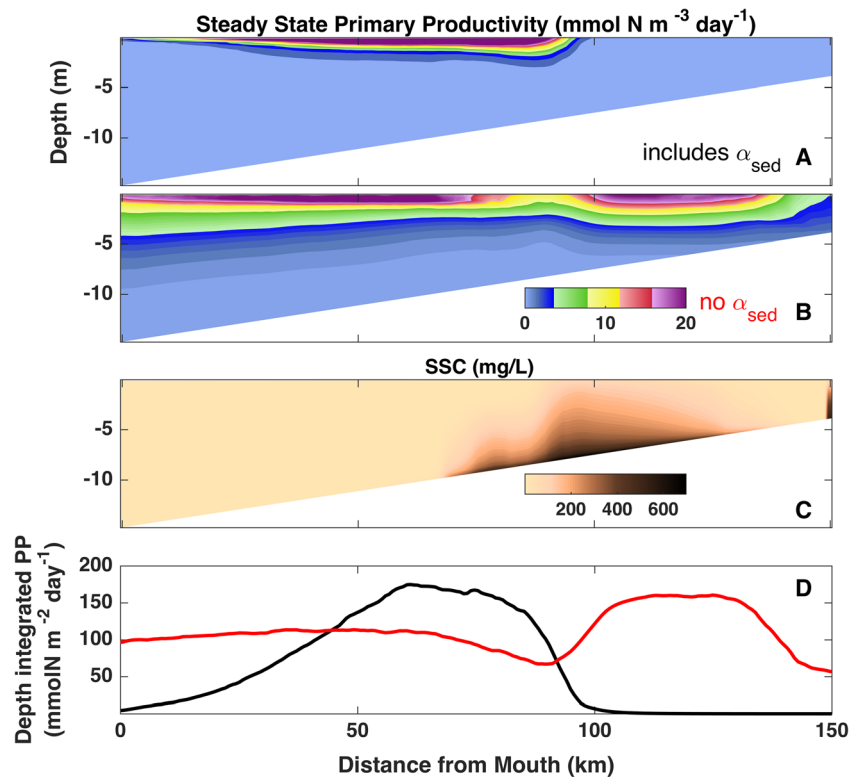
Similar to the spring-neap variability of stratification seen in the model (Fig. 11), the Delaware Estuary becomes significantly stratified during neap tides (Fig. 12). Since the Delaware Estuary has been previously characterized as well-mixed (Beardsley and Boicourt 1981; Garvine et al. 1992; Janzen and Wong 2002), observations of such strong stratification provide supporting context that the model results (Fig. 11) capture realistic dynamics. Figure 12b shows the stratification conditions at a mooring site in the vicinity of the ETM over a spring-neap cycle in July 2011. During the spring tides (shaded in gray), the site is fairly well-mixed with slight stratification developing on a tidal timescale. During neap tide however, there is a salinity difference of roughly 10 psu between the surface and bottom. Looking at three cross-sections during neap tide 26 July 2011 (Fig. 12c–h), it is evident that the estuary is strongly stratified. The optical backscatter signal, a proxy for sediment concentration, indicates that sediment is mixed to the surface where stratification is weak but is prevented from reaching the surface in more strongly stratified areas. We note that the optical backscatter signal at km 7 in Fig. 12e may be capturing chlorophyll biomass that is similar in size to sediment particles. Generally, the chlorophyll maxima spatially coincide with areas of strong stratification and low surface sediment, and the blooms are constrained to the surface layer by stratification. These observations provide further evidence that the model result are realistic and also suggest that spring-neap variability can modulate stratification even under conditions of constant river

Fig. 12 a Map of the mooring location (*black dot*) and three cross-channel sections (*blue dots*). Bathymetry is contoured in *gray*. **b** Depth-averaged velocity (*black line*, m s^{-1}) and surface (*red line*) and bottom (*blue line*) salinity from the mooring shown by *black dot* in **a**. The spring tide is shaded *gray*, the neap tide is *white*. **c–h** Observations from the three cross-channel sections 26 July 2011 (**c** and **d**, **e** and **f**, and **g** and **h** correspond with labels *c*, *e*, and *g* respectively in **a**. The *brown shading* is optical back-scatter, a proxy for sediment (**c**, **e**, **g**, volts), the *green shading* is chlorophyll concentrations (**d**, **f**, **h**, μg L^{-1}) and the *black contours* are salinity (psu)
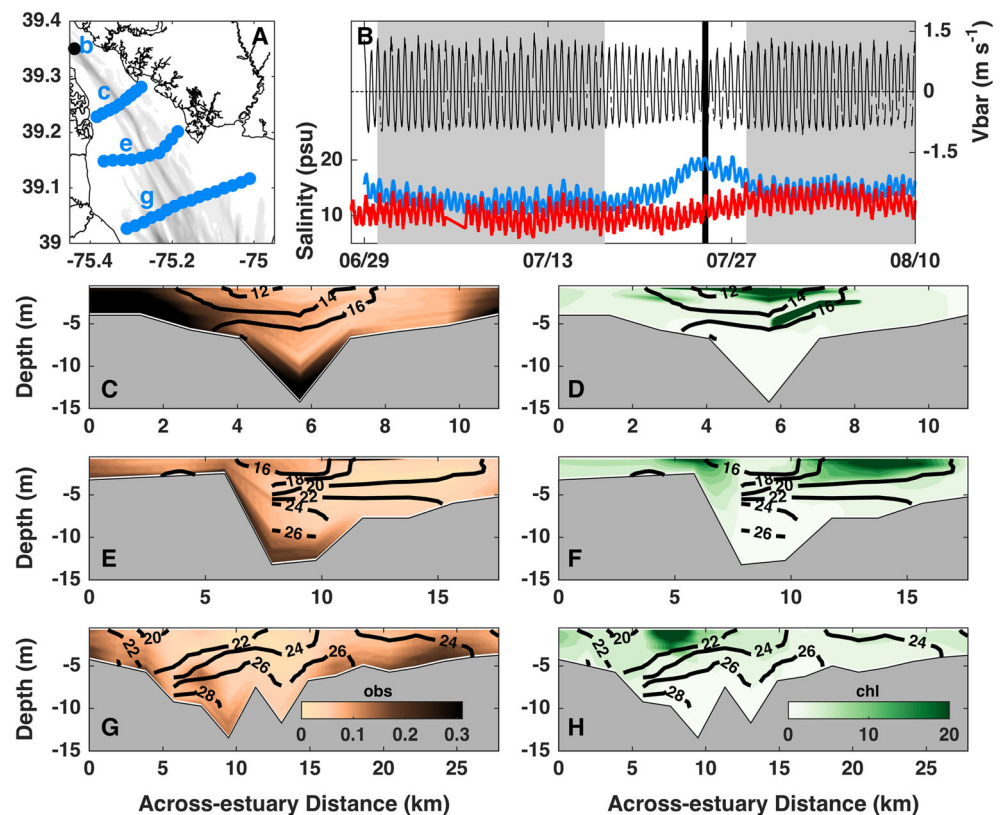
discharge, which significantly impacts suspended-sediment concentration (Sommerfield and Wong 2011) and by extension productivity.

While the distribution of chlorophyll and sediment is predominantly controlled by along-channel processes, the cross-sectional observations (Fig. 12) hint that the chlorophyll blooms may have lateral structure related to lateral stratification and sediment features (McSweeney et al. 2016). These observations provide motivation to study the three-dimensional nature of sediment impacts on light-limited productivity in future work.

Implications for Modeling Primary Productivity

In order to contextualize the importance of sediment absorption of light, we run the model with and without the sediment absorption included in the total light attenuation. Figure 13 shows the average primary production (mmol N m^{-3} day^{-1}) for the river discharge 75 m^3 s^{-1} case (M2 only) where only Eq. 4 is altered. When light attenuation by sediment is accounted for, we see production at the surface down-estuary of the ETM and no production where sediment is resuspended to the surface. When sediment is in the model but not attenuating light, production is spread along the estuary (Fig. 13b). Comparing the two spatial patterns in Fig. 13 with observations of chlorophyll and nitrate (Fig. 3), it is evident that sediment

attenuation can play a key role in controlling the spatial distribution of productivity.

This result highlights the importance of including both sediment and light attenuation by sediment in biogeochemical models of turbid estuaries. Models that do not account for sediment attenuation will miss key light limitations and thus overestimate the levels of primary productivity that can be supported. Figure 11c suggests that the overestimations may be especially important up- and down-estuary of the true bloom location. There is an increasing amount of evidence that modeling light absorption in coastal and estuarine systems should be of high importance (Desmit et al. 2005; Arndt et al. 2007), and yet these linkages are poorly represented in many biogeochemical models. Our study provides further evidence that the linkages between hydrodynamics, suspended sediment, light, and productivity are important, emphasizing that stratification is key to understanding how these processes are interconnected. Since stratification can vary on tidal and seasonal timescales, it is important to consider the effects of both river discharge and spring-neap variability of light limitation.

As noted in the "Idealized Model" section, we also ran the model with two different α_{sed} values, 0.065 and 0.075 m^{-1}/(mg L.$^{-1}$), to evaluate the model's sensitivity to α_{sed}. The model output for the two sediment attenuation values did not vary significantly. The spatial patterns described were similar, with a slight impact on the

magnitudes of production and chlorophyll concentration. Because the attenuation coefficient is estimated from the relationship between sediment and light, it is possible that the difference between our estimation and that of Pennock (1985) is indicative of a temporal shift in the properties of the sediment. A study of the Rhode River, a tributary of the Chesapeake Estuary, concluded that a shift toward smaller, organic particles impacted water clarity despite similar SSC concentrations (Gallegos et al. 2005). Further work would be needed to determine if a shift in sediment size such as that observed in the Rhode River is happening in the Delaware or if the variability is merely a result of the observational time periods capturing different ETM ratios of biogenic and mineral material. For example, biomarker and stable isotope carbon analysis of samples from these cruises indicate that discharge in the winter and spring delivers higher levels of terrestrial matter (Hermes 2013), which would impact the sediment-specific absorption. Regardless, based on our model sensitivity runs, we conclude that the impacts of sediment on light-limitation patterns are relatively insensitive to the observed variations in α_{sed} compared to the sensitivity to sediment concentration.

Conclusions

Sediment resuspension and concentration play an important role in limiting light-availability and primary production in turbid estuaries. The Delaware Estuary is a high-nutrient, low-growth environment whose water quality is thought to be largely controlled by sediment attenuation of light. This study uses observations from eight along-estuary surveys and an idealized ROMS model to focus on the interactions between the ETM, light limitation, and productivity, emphasizing the role of stratification and sediment dynamics. While the location of the ETM is largely controlled by river discharge, the ETM structure is controlled by stratification due to both river inflow and spring-neap variability. The leading edge of the ETM tends to follow the salt intrusion front and is characterized by resuspension that spans the entire water column, compared to the tail of the ETM which is confined below the surface mixed layer by stratification. We observe that the depth of the 1% light level is primarily controlled by this structure and thus shallows in the vicinity of the ETM where resuspension reaches the surface. Consequently, production is minimal in the ETM region due to light limitations, and chlorophyll concentrations are maximal down-estuary of the turbidity maximum.

The location and structure of the turbidity maximum varies with river discharge, causing notable seasonal variability of the sediment and chlorophyll spatial patterns. Surface sediment concentrations in the ETM region are maximal in March and December due to the delivery of sediment by high river flows. However, despite the similar ETM features, the along-channel distribution of chlorophyll differs in the winter and spring. In the spring, stratification induced by higher river discharge limits resuspension to lower in the water column and phytoplankton blooms can be initiated in the surface mixed layer. In the winter months, well-mixed conditions and reduced sunlight create conditions less conducive to productivity.

Our results highlight that both high river flows and neap tides can drive stratification that is sufficient to prevent suspended sediment from reaching the surface, thus creating light conditions favorable for primary production. Previous studies have classified Delaware to be well-mixed, such that light limitation is a persistent control on production except for in cases on increased river run-off (Pennock and Sharp 1986). Here, we suggest that even in low river discharge conditions, stratification can persist under neap tides and thereby limit sediment from being resuspended into the surface layer.

We ran an idealized ROMS model with the diffuse attenuation coefficients including and excluding the attenuation by sediment to isolate the contribution of sediment attenuation to the spatial patterns of productivity. From this model comparison, we conclude that the absorption of light by surface sediment is an extremely important factor that controls the spatial distributions of productivity, chlorophyll, nitrate, and oxygen that are observed in high-nutrient, low-growth turbid estuaries Therefore, we posit that biogeochemical models of urbanized turbid estuaries may grossly overestimate productivity and miss important spatiotemporal patterns if they do not account for the suspended sediment attenuation of light.

While our analysis focuses on observations from the Delaware Estuary and a complementary model, the mechanisms discussed in this paper are broadly applicable to turbid estuaries with an excess of nutrients. Since the salinity front modulates the location of the ETM, an estuary's along-channel sediment distribution will respond to river discharge changes, which are predictably seasonal in most systems. Furthermore, because estuarine stratification is known to increase with neap tides and strong river flows, resuspended sediment within an ETM may not reach the surface during these conditions. Since the magnitude and duration of stratification are key factors to whether sediment is resuspended to the surface layer, the relative importance of both river discharge and spring-neap variability may vary from system to system. In some estuaries, high river flow can push the salt field out of the system entirely, in which case the entire estuary would become fresh and likely turbid at the surface due to the lack of stratification. Or, even if the salt field remains in the estuary, the stratified region can be shortened significantly and the flushing time would be too great for chlorophyll biomass to accumulate within the stratified region.

Another factor to consider in this paradigm is the size and sinking velocity of the sediment types. For example, the

described mechanisms may be confounded in certain cases, such as a river discharge event that delivers extremely fine sediment. If the sinking velocities are low enough and the estuary becomes strongly stratified, the increased sediment load could become trapped at the surface by stratification. In that scenario, stratified conditions would coincide with increased light attenuation by sediment and a poor environment for production. Therefore, the conclusion that stratification plays an important role in modulating sediment concentrations at the surface and light-availability is robust, but the implications of this mechanism can impact estuarine systems differently.

References

Aristizábal, M., and Chant, R. 2013. A numerical study of salt fluxes in Delaware Bay Estuary, Journal of Physical Oceanography.

Aristizábal, M., and R. Chant. 2014. Mechanisms Driving Stratification in Delaware Bay Estuary. *Ocean Dynamics* 64: 1615–1629.

Arndt, S., J.P. Vanderborght, and P. Regnier. 2007. Diatom growth response to physical forcing in a macrotidal estuary: coupling hydrodynamics, sediment transport, and biogeochemistry. *Journal of Geophysical Research: Oceans* 112.

Beardsley, R.C., and W.C. Boicourt. 1981. On estuarine and continental-shelf circulation in the Middle Atlantic Bight. *Evolution of physical oceanography* 198-233.

Biggs, R.B., J.H. Sharp, T.M. Church, and J.M. Tramontano. 1983. Optical properties, suspended sediments, and chemistry associated with the turbidity maxima of the Delaware Estuary. *Canadian Journal of Fisheries and Aquatic Sciences* 40: s172–s179.

Biggs, R.B., and E.L. Beasley. 1988. Bottom and suspended sediments in the Delaware River and Estuary. *Ecology and Restoration of the Delaware River Basin* 116-131.

Burchard, H., R.D. Hetland, E. Schulz, and H.M. Schuttelaars. 2011. Drivers of residual estuarine circulation in tidally energetic estuaries: Straight and irrotational channels with parabolic cross section. *Journal of Physical Oceanography* 41: 548–570.

Cloern, J.E. 1991. Tidal stirring and phytoplankton bloom dynamics in an estuary. *Journal of marine research* 49: 203–221.

Cook, T.L., C.K. Sommerfield, and K.-C. Wong. 2007. Observations of tidal and springtime sediment transport in the upper Delaware Estuary, Estuarine. *Coastal and Shelf Science* 72: 235–246.

De Swart, H., H. Schuttelaars, and S. Talke. 2009. Initial growth of phytoplankton in turbid estuaries: A simple model. *Continental Shelf Research* 29: 136–147.

Desmit, X., J.-P. Vanderborght, P. Regnier, and R. Wollast. 2005. Control of phytoplankton production by physical forcing in a strongly tidal, well-mixed estuary. *Biogeosciences* 2: 205–218.

Devlin, M., J. Barry, D. Mills, R. Gowen, J. Foden, D. Sivyer, and P. Tett. 2008. Relationships between suspended particulate material, light attenuation and Secchi depth in UK marine waters, Estuarine. *Coastal and Shelf Science* 79: 429–439.

Duval, D. 2013. Sedimentary response of the Delaware Estuary to tropical cyclones Irene and Lee in 2011, University of Delaware.

Fennel, K., J. Wilkin, J. Levin, J. Moisan, J. O'Reilly, and D. Haidvogel. 2006. Nitrogen cycling in the Middle Atlantic Bight: Results from a three-dimensional model and implications for the North Atlantic nitrogen budget. *Global Biogeochemical Cycles* 20.

Fisher, T.R., L.W. Harding, D.W. Stanley, and L.G. Ward. 1988. Phytoplankton, nutrients, and turbidity in the Chesapeake, Delaware, and Hudson estuaries, Estuarine. *Coastal and Shelf Science* 27: 61–93.

Gallegos, C.L., T.E. Jordan, A.H. Hines, and D.E. Weller. 2005. Temporal variability of optical properties in a shallow, eutrophic estuary: Seasonal and interannual variability, Estuarine. *Coastal and Shelf Science* 64: 156–170.

Ganju, N., J. Miselis, and A. Aretxabaleta. 2014. Physical and biogeochemical controls on light attenuation in a eutrophic, back-barrier estuary. *Biogeosciences* 11: 7193–7205.

Garvine, R.W., R.K. McCarthy, and K.-C. Wong. 1992. The axial salinity distribution in the Delaware estuary and its weak response to river discharge, Estuarine. *Coastal and Shelf Science* 35: 157–165.

Gibbs, R.J., L. Konwar, and A. Terchunian. 1983. Size of flocs suspended in Delaware Bay. *Canadian Journal of Fisheries and Aquatic Sciences* 40: s102–s104.

Haidvogel, D.B., H.G. Arango, K. Hedstrom, A. Beckmann, P. Malanotte-Rizzoli, and A.F. Shchepetkin. 2000. Model evaluation experiments in the North Atlantic Basin: simulations in nonlinear terrain-following coordinates. *Dynamics of Atmospheres and Oceans* 32: 239–281.

Hansen, D.V., and M. Rattray. 1965. Gravitational circulation in straits and estuaries. *Journal of Marine Research* 23.

Hermes, A. L. 2013. Spatial and seasonal particulate organic carbon cycling within the Delaware estuary, assessed using biomarker and stable carbon isotopic approaches, Rutgers University-Graduate School-New Brunswick.

Janzen, C.D., and K.C. Wong. 2002. Wind-forced dynamics at the estuary-shelf interface of a large coastal plain estuary. *Journal of Geophysical Research: Oceans (1978–2012)* 107 .2-1-2-12

Ketchum, B. H. 1952. The distribution of salinity in the estuary of the Delaware River, Woods Hole Oceanographic Institution.

Kineke, G., and R. Sternberg. 1992. Measurements of high concentration suspended sediments using the optical backscatterance sensor. *Marine Geology* 108: 253–258.

Lawson, S., P. Wiberg, K. McGlathery, and D. Fugate. 2007. Wind-driven sediment suspension controls light availability in a shallow coastal lagoon. *Estuaries and Coasts* 30: 102–112.

MacCready, P., and W.R. Geyer. 2010. Advances in estuarine physics. *Annual Review of Marine Science* 2: 35–58.

Malone, T., L. Crocker, S. Pike, and B. Wendler. 1988. Influences of river flow on the dynamics of phytoplankton production in a partially stratified estuary, Marine ecology progress series. *Oldendorf* 48: 235–249.

Mansue, L. J., and Commings, A. B. 1974. Sediment transport by streams draining into the Delaware Estuary, US Government Printing Office.

Marchesiello, P., J.C. McWilliams, and A. Shchepetkin. 2001. Open boundary conditions for long-term integration of regional oceanic models. *Ocean modelling* 3: 1–20.

May, C.L., J.R. Koseff, L.V. Lucas, J.E. Cloern, and D.H. Schoellhamer. 2003. Effects of spatial and temporal variability of turbidity on phytoplankton blooms. *Marine Ecology Progress Series* 254: 111–128.

McSweeney, J.M., R. Chant, and C.K. Sommerfield. 2016. Lateral Variability of Sediment Transport in the Delaware Estuary. *Journal of Geophysical Research: Oceans* 121: 725–744. doi:10.1002/2015 JC010974.

Monismith, S.G., W. Kimmerer, J.R. Burau, and M.T. Stacey. 2002. Structure and flow-induced variability of the subtidal salinity field in northern San Francisco Bay. *Journal of Physical Oceanography* 32: 3003–3019.

Nash, D. B. 1994. Effective sediment-transporting discharge from magnitude-frequency analysis, The Journal of Geology, 79-95.

Neiheisel, J. 1973. Source of detrital heavy minerals in estuaries of the Atlantic Coastal Plain.

Orlanski, I. 1976. A simple boundary condition for unbounded hyperbolic flows. *Journal of computational physics* 21: 251–269.

Pennock, J.R. 1985. Chlorophyll distributions in the Delaware estuary: regulation by light-limitation, Estuarine. *Coastal and Shelf Science* 21: 711–725.

Pennock, J.R., and J.H. Sharp. 1986. Phytoplankton production in the Delaware Estuary: temporal and spatial variability. *Marine Ecology Progress Series* 34: 143–155.

Pennock, J.R. 1987. Temporal and spatial variability in phytoplankton ammonium and nitrate uptake in the Delaware Estuary, Estuarine. *Coastal and Shelf Science* 24: 841–857.

Pennock, J.R., and J.H. Sharp. 1994. Temporal alternation between light- and nutrient-limitation of phytoplankton production in a coastal plain estuary, Marine ecology progress series. *Oldendorf* 111: 275–288.

Ralston, D.K., W.R. Geyer, and J.C. Warner. 2012. Bathymetric controls on sediment transport in the Hudson River estuary: Lateral asymmetry and frontal trapping. *Journal of Geophysical Research: Oceans (1978–2012)* 117.

Scully, M.E., and C.T. Friedrichs. 2007. Sediment pumping by tidal asymmetry in a partially mixed estuary. *Journal of Geophysical Research: Oceans (1978–2012)* 112.

Sharp, J.H., C.H. Culberson, and T.M. Church. 1982. The chemistry of the Delaware estuary. General considerations. *Limnology and Oceanography* 27: 1015–1028.

Sharp, J.H., J.R. Pennock, T.M. Church, J.M. Tramontano, and L.A. Cifuentes. 1984. *The estuarine interaction of nutrients, organics, and metals: A case study in the Delaware Estuary, in: The Estuary as a Filter*, 241–258. New York: Academic Press.

Sharp, J.H., L.A. Cifuentes, R.B. Coffin, J.R. Pennock, and K.-C. Wong. 1986. The influence of river variability on the circulation, chemistry, and microbiology of the Delaware Estuary. *Estuaries* 9: 261–269.

Sharp, J.H., K. Yoshiyama, A.E. Parker, M.C. Schwartz, S.E. Curless, A.Y. Beauregard, J.E. Ossolinski, and A.R. Davis. 2009. A biogeochemical view of estuarine eutrophication: Seasonal and spatial trends and correlations in the Delaware Estuary. *Estuaries and coasts* 32: 1023–1043.

Shchepetkin, A.F., and J.C. McWilliams. 2005. The regional oceanic modeling system (ROMS): a split-explicit, free-surface, topography-following-coordinate oceanic model. *Ocean Modelling* 9: 347–404.

Simpson, J.H., J. Brown, J. Matthews, and G. Allen. 1990. Tidal straining, density currents, and stirring in the control of estuarine stratification. *Estuaries* 13: 125–132.

Sommerfield, C. K., and Madsen, J. A. 2004. Sedimentological and Geophysical Survey of the Upper Delaware Estuary: Final Report to the Delaware River Basin Commission, University of Delaware Sea Grant Publication, 126 pp.

Sommerfield, C.K., and K.C. Wong. 2011. Mechanisms of sediment flux and turbidity maintenance in the Delaware Estuary. *Journal of Geophysical Research: Oceans (1978–2012)* 116.

Stacey, M.T., J.R. Burau, and S.G. Monismith. 2001. Creation of residual flows in a partially stratified estuary. *J. Geophys. Res* 106: 013–017.

Stross, R.G., and R.C. Sokol. 1989. Runoff and flocculation modify underwater light environment of the Hudson River estuary, Estuarine. *Coastal and Shelf Science* 29: 305–316.

Umlauf, L., and H. Burchard. 2003. A generic length-scale equation for geophysical turbulence models. *Journal of Marine Research* 61: 235–265.

US Census. 2010. Population Change for Metropolitan and Micropolitan Statistical Areas in the United States and Puerto Rico, http://www.census.gov/population/www/cen2010/cph-t/cph-t-5.html.

Warner, J.C., C.R. Sherwood, R.P. Signell, C.K. Harris, and H.G. Arango. 2008. Development of a three-dimensional, regional, coupled wave, current, and sediment-transport model. *Computers & Geosciences* 34: 1284–1306.

Weil, C. B. 1977. Sediments, structural framework, and evolution of Delaware Bay, a transgressive estuarine delta, Sea Grant Technical Report.

Wofsy, S. 1983. A simple model to predict extinction coefficients and phytoplankton biomass in eutrophic waters. *Limnology and Oceanography* 28: 1144–1155.

Yoshiyama, K., and J.H. Sharp. 2006. Phytoplankton response to nutrient enrichment in an urbanized estuary: Apparent inhibition of primary production by overeutrophication. *Limnology and Oceanography* 51: 424–434.